

MedBridge: Bridging Foundation Vision-Language Models to Medical Image Diagnosis in Chest X-Ray

Yitong Li*, Morteza Ghahremani*, Christian Wachinger

Lab for AI in Medical Imaging, Technical University of Munich (TUM), Germany
Munich Center for Machine Learning (MCML), Germany

Abstract

Recent vision-language foundation models deliver state-of-the-art results in natural image classification, but falter in medical images due to pronounced domain shifts. Training a medical foundation model also requires substantial resources, including extensive annotated data and high computational capacity. To bridge this gap with minimal overhead, we introduce MedBridge, a lightweight multimodal adaptation framework that flexibly re-purposes arbitrary pre-trained foundation VLMs for medical image diagnosis. MedBridge comprises three novel core components. First, a Focal Sampling module that subsamples and extracts high-resolution local regions to capture subtle pathological features, compensating for the limited input resolution of foundation VLMs. Second, a Query-Encoder model with a small set of learnable queries to align the feature maps of frozen VLMs with medical semantics, without requiring retraining of the backbone layers. Third, a Mixture of Experts mechanism, driven by learnable queries, harnesses the complementary strength of various VLMs to maximize diagnostic performance. We evaluate MedBridge on five chest radiograph benchmarks in three key adaptation tasks, demonstrating its superior performance in both cross-domain and in-domain adaptation settings under varying levels of training data availability. MedBridge achieved an improvement of 6-15% in AUC compared to state-of-the-art VLM adaptation methods in multi-label thoracic disease diagnosis, underscoring its effectiveness in leveraging diverse foundation models for accurate and data-efficient medical diagnosis. Our project and code are available at <https://github.com/ai-med/MedBridge>.

1. Introduction

Recent foundation vision-language models (VLMs) have gained substantial capabilities through large-scale pre-training on extensive datasets covering both visual and tex-

tual modalities [6, 17, 18, 25, 40, 44]. This pre-training paradigm enables the models to learn rich, transferrable cross-modal representations essential for a wide variety of downstream tasks [1, 13, 31, 39]. As these VLMs continue to grow in size, full fine-tuning of all parameters for a specific downstream task becomes computationally intensive and elevates the risk of overfitting. Hence, recent research has focused on developing parameter-efficient transfer learning strategies to effectively adapt these large-scale models to downstream tasks across diverse photographic image datasets [5, 7, 9, 41, 42, 52, 53, 55].

Despite these recent advances, adapting foundation VLMs to *medical* imaging remains challenging due to significant domain discrepancies. Medical images are structurally and semantically distinct from the natural images used for pretraining: they exhibit consistent anatomical layouts and subtle pathological features. While natural image tasks rely heavily on high-level object cues, medical diagnosis often hinges on holistic, fine-grained features dispersed across the image, which necessitates high-resolution input to preserve critical details. Compounding this issue, the default input resolution of most foundation VLMs, i.e., 224×224 , is insufficient to capture the detailed cues in medical images, such as chest X-rays, which typically exceed 2048×2048 pixels. Although recent efforts have begun leveraging foundation VLMs for preliminary medical tasks such as anomaly detection [11, 48], segmentation [23, 49], and object detection [24], the challenge of achieving a flexible and efficient adaptation of various pre-trained foundation VLMs for diagnosis, a core clinical task, remains largely unaddressed. This challenge is further amplified by the multi-label nature of medical diagnosis, where a single image often corresponds to several co-existing disease labels indicated by multiple pathological cues [10]. However, existing VLM adaptation techniques are primarily designed for single-label natural image classification and do not transfer well to medical diagnosis, as shown in Fig. 1b.

To address these challenges, we propose *MedBridge*, a lightweight domain adaptation framework that can flexibly

*Equal Contribution.

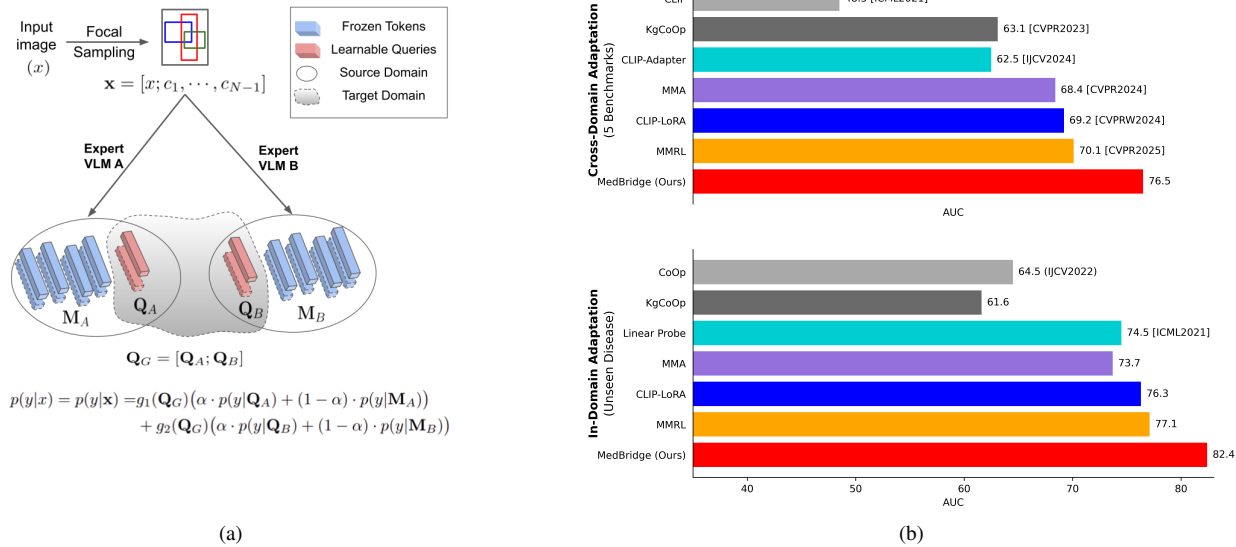


Figure 1. (a) To predict the label(s) of an image x , i.e., $p(y|x)$, MedBridge operates in three stages. In the first stage, it expands the visual observations from a single image x to N images \mathbf{x} through a focal sampling module. We then introduce a mixture of experts (MoE), where experts are frozen foundation VLMs. Each expert produces a set of \mathbf{M} tokens for the input image, and simultaneously generates a set of \mathbf{Q} learnable queries that interact with frozen tokens, where Expert $A : \{\mathbf{M}_A, \mathbf{Q}_A\}$ and Expert $B : \{\mathbf{M}_B, \mathbf{Q}_B\}$. A gating network g , trained on learnable queries $\mathbf{Q}_G = [\mathbf{Q}_A, \mathbf{Q}_B]$, dynamically weights the experts, allowing prioritization of different components. The final prediction is a combination of the visual tokens \mathbf{M} and the learnable queries \mathbf{Q} , modulated by α . The learnable queries $\{\mathbf{Q}_A, \mathbf{Q}_B\}$ add approximately 4% more parameters compared to the base models, but they efficiently help guide the MoE toward the target domain’s representation. (b) MedBridge yields significant improvements in disease classification across various medical benchmarks.

adapt arbitrary foundation VLMs for accurate medical image diagnosis in a resource-efficient manner (Fig. 1a). MedBridge’s design introduces minimal additional parameters, reducing computational overhead and reducing overfitting risks. It enables both cross-domain adaptation from various general-purpose VLMs, including CLIP [25], LLaVa [18], and further refinement of pre-trained medical ones like CheXzero [33], MedGemma [27], maintaining strong performance even with limited training data. Across five benchmark medical datasets for multi-label thoracic disease classification, MedBridge consistently outperforms diverse state-of-the-art adaptation methods, offering substantial advantages through improved accuracy, reduced computational costs, and robust performance under different adaptation scenarios (Fig. 1b). Our key contributions are:

- A Focal Sampling module to maintain the high resolution of the original input image in local regions, enabling the detection of subtle pathological signals.
- A generic Query-Encoder (QEncoder) that bridges the wide domain gap between foundation VLMs and medical images with limited learnable queries.
- A Mixture of Experts (MoE) integration on the learnable queries of QEncoders to dynamically combine the strength of multiple foundation VLMs.
- The demonstration of MedBridge’s robust performance for bridging different VLMs to the medical domain on five medical datasets and three adaptation tasks.

2. Related Work

Vision-language models. Recent VLMs like CLIP [25], LLaVA [18], SigLIP [44], OpenCLIP [6], Gemini [8], and Gemma [32] have made significant progress by leveraging large-scale training on massive datasets with billions of image-text pairs [26], achieving strong performance across diverse downstream tasks. However, their direct deployment in the medical domain remains limited, e.g., CLIP in Fig. 1b, due to a substantial domain shift [29, 33, 51], necessitating further domain-specific adaptation.

Parameter-efficient transfer learning for VLMs. As VLMs scale, fine-tuning all model parameters becomes computationally expensive, prone to overfitting or catastrophic forgetting. To address this, recent work has focused on parameter-efficient transfer learning, primarily through prompt learning and adapter-based methods. In prompt learning approaches, CoOp [53] replaces fixed templates with learnable vectors, CoCoOp [52] generates instance-specific prompts with visual features, while ProGrad [55] and KgCoOp [42] aim to retain pre-trained knowledge during adaptation. Recent adapter-based methods introduce lightweight modules into the network, in which CLIP-Adapter [7] refines representations using MLP-based adapters, Tip-Adapter [46] enables test-time inference via feature caching, MMA [41] and MMRL [9] both incorporate a shared space to facilitate multimodal interaction. CLIP-LoRA [43] employs the low-rank adaptation

for VLMs. These adaptation strategies are primarily tailored for in-domain, cross-dataset generalization and may not transfer well to cross-domain medical data as shown in Fig. 1b. In contrast, with MedBridge we aim to go beyond conventional adapters by explicitly addressing domain discrepancies, enabling robust domain adaptation from foundation VLMs to the medical data space.

Adaptation of foundation VLMs to the medical domain. Recent studies have extended pre-trained general-purpose VLMs to medical domain for report generation [20, 21], anomaly detection [11, 48], segmentation [23, 49], reconstruction [4], and object detection [24], achieving promising results. However, to the best of our knowledge, a flexible adaptation of different general-purpose VLMs for disease diagnosis is largely underexplored. Current efforts mostly either carry out additional large-scale VLM pre-training to build medical-specific foundation models [54], e.g., GLO-RIA [12], ConVIRT [50], MedCLIP [36], CheXzero [33], KAD [47], MedKLIP [37], MGCA [34], MAVL [22], and MedGemma [27], which demands substantial computational resources, or adaptation of VLMs that have already been pre-trained on medical data [16, 29, 45]. However, our goal is to design a lightweight and flexible domain adaptation approach that can rapidly re-purpose arbitrary foundation VLMs or refine pre-trained medical ones for unseen disease diagnosis, eliminating the heavy overhead of full re-training while maintaining strong clinical performance.

3. Proposed Method

Let s and t denote the source and target domains, and K the number of ViT-based foundation VLM backbones pre-trained in the source image domain. Our goal is to adapt them for multi-label disease classification on the chest X-ray data $\mathcal{D}_t = \{(x_t^i, y_t^i)\}_{i=1}^{N_t}$, where each image $x_t \in \mathbb{R}^{H \times W \times 3}$ is annotated with ground-truth disease labels $y_t \in \{0, 1\}^L$, indicating the presence of L possible diseases: each component $y_{t,j} = 1$ if the j -th disease is present and 0 otherwise. y_t will be converted into a list of textual prompts in the template of ‘a radiology image with [CLASS]’, and then encoded by a text encoder. When paired clinical reports r_t are available, we extend the target set to $\mathcal{D}_t = \{(x_t^i, y_t^i, r_t^i)\}_{i=1}^{N_t}$, incorporating r_t as auxiliary supervision during adaptation.

MedBridge is designed as a lightweight domain adapter to bridge arbitrary foundation VLMs for the purpose of medical image diagnosis, i.e., $p(y_t|x_t)$. The proposed architecture is shown in Fig. 2, containing three key modules: 1) a Focal Sampling module extracting high-resolution local regions from original input medical images to capture fine-grained pathological cues and enhance the representation robustness; 2) a Query-Encoder (QEncoder) module on top of each VLM encoder, encoding each input into tokens

with frozen backbones and generating a small set of learnable queries to enable parameter-efficient domain adaptation; and 3) a Mixture of Experts (MoE) module receiving query-augmented tokens and dynamically selecting specialized VLM encoders to improve scalability without computational overhead. The details of each component are provided below.

Focal Sampling: *One image contains the richness of thousands*, especially in medical imaging, where disease manifestations can appear as multiple small and subtle regions, which may vanish when images are down-scaled to the default input size expected by most foundation VLMs. To better preserve detailed pathological cues, we introduce a focal sampling strategy, which augments the resized input image with multiple fine-grained local patches. From each high-resolution X-ray image, we extract ‘ $N - 1$ ’ small local regions via either random selection or a sliding window with overlap, and stack them alongside the resized full image to create an N -view input. We later apply self-attention over the N image embeddings to capture their contextual relationships and derive candidate tokens. This strategy enhances the visibility of disease-related regions and reduces the model’s sensitivity to precise image alignments, ensuring more robust detection regardless of slight variations in positioning. It also acts as an implicit ensemble, expanding spatial coverage while mitigating overfitting and overdependence on specific image regions.

Query-Encoder (QEncoder): The QEncoder adds Q learnable queries $\mathbf{Q} = \{q_i\}_{i=1}^Q$ to interact with the M frozen tokens $\mathbf{M} = \{m_i\}_{i=1}^M$ from foundation VLMs, aiming to reduce the gap in representation between the source and target domains. Due to interactions with the frozen tokens, the auxiliary queries are enriched with contextual content. Concurrently, these auxiliary queries are trained specifically on the target task, enabling them to learn features pertinent to the target domain, while we keep their dimension smaller than the foundation models. As depicted in Fig. 2, the QEncoder keeps all n layers of the foundation VLM encoder frozen. After the first n_1 layers, it generates and injects Q learnable query tokens, initialized with a normal distribution $\mathcal{N}(0, 0.02)$, and then stacks them on the foundation tokens. The concatenated tokens are processed through the rest n_2 encoder layers ($n_2 = n - n_1$), interacting with each other through attention mapping:

$$\begin{aligned} \mathbf{Z}^i &= [\mathbf{M}^i; \mathbf{Q}^i] + \text{MHSA}(\text{Norm}([\mathbf{M}^i; \mathbf{Q}^i])), \\ [\mathbf{M}^{i+1}; \mathbf{Q}^{i+1}] &= \mathbf{Z}^i + \text{FFN}(\text{Norm}(\mathbf{Z}^i)), \\ i &= n_1 + 1, \dots, n_1 + n_2 \end{aligned} \quad (1)$$

where MHSA and FFN denote the multi-head self-attention and feed-forward network in the VLM backbones, respectively, and Norm the layer normalization [2]. It is worth noting that QEncoder differs from QFormer [15]. In QFormer,

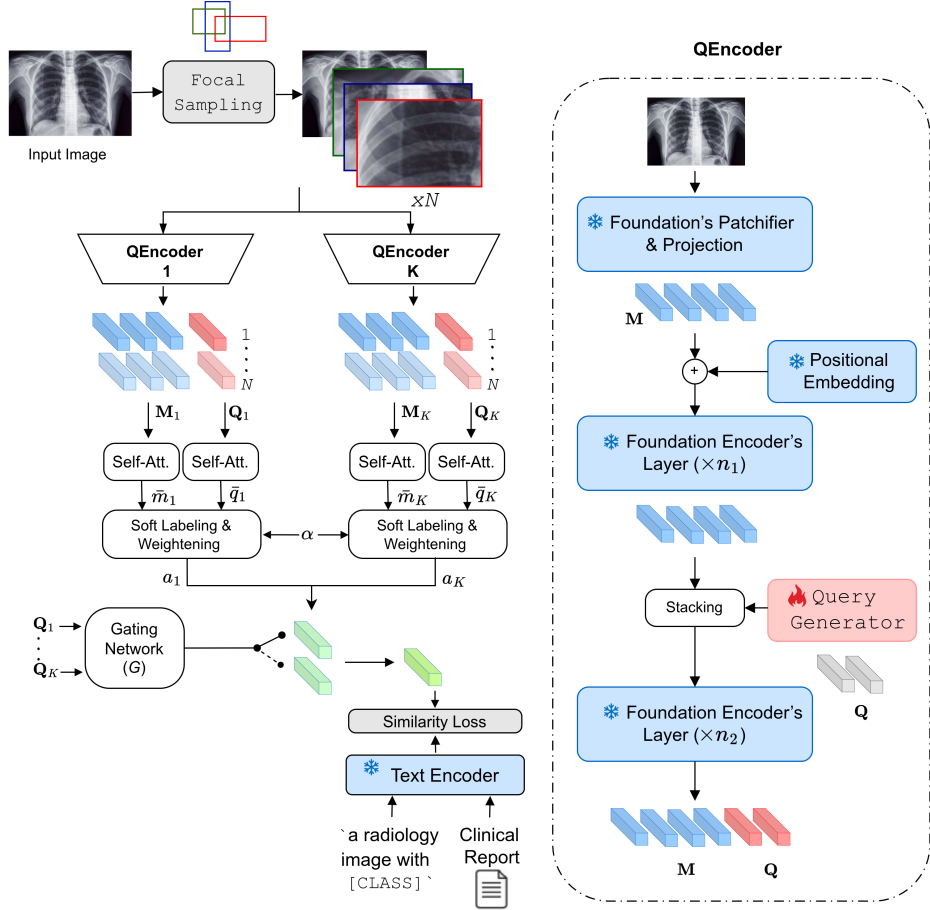


Figure 2. *MedBridge* framework: Focal sampling extracts fine-grained regions from the high-resolution input image, encoded by QEncoders into frozen tokens and learnable queries for lightweight adaptation. A Mixture of Experts (MoE) module routes these tokens through the most relevant encoders, and the final prediction combines soft labels from both query and frozen tokens with weight α .

the learnable queries first interact with one another through self-attention layers and then interact with image features via cross-attention layers, where the tokens from the vision encoder serve as keys and values. Additionally, these queries interact with text through the corresponding layers of self-attention.

As the input consists of N associated images from the focal sampling, there exist correspondingly N frozen token sets \mathbf{M} and N trainable query token sets \mathbf{Q} per encoder, respectively. We apply a self-attention to extract contextual relationships within N images and then a max-pooling to extract the candidate tokens, i.e., $\{\bar{m}_k\}_{k=1}^K$ for frozen tokens and $\{\bar{q}_k\}_{k=1}^K$ for learnable query tokens from K experts. Each expert produces an output class token a_k , which is obtained through a softening of the frozen feature and query tokens:

$$a_k = \alpha \cdot \bar{q}_k + (1 - \alpha) \cdot \bar{m}_k, \quad k = 1, \dots, K \quad (2)$$

where α is a constant hyperparameter that determines the contribution of the query token set to the resulting class token. An ablation study exploring this hyperparameter is presented in Sec. 4.2.

Mixture of Experts (MoE): The MoE takes the learnable queries $\mathbf{Q}_k \in \mathbb{R}^{N \times Q \times f}$, $k = 1, \dots, K$, where f denotes the embedding dimension, from K expert encoders as input to a gating network G , which dynamically computes and weights the contribution of each expert. Given an input token set $\mathbf{Q}_G = \{\mathbf{Q}_k\}_{k=1}^K$, the gating network computes a weight vector $\mathbf{g}(\mathbf{Q}_G) = [g_1(\mathbf{Q}_G), g_2(\mathbf{Q}_G), \dots, g_K(\mathbf{Q}_G)]$, where each weight $g_k(\mathbf{Q}_G)$ is obtained via a softmax layer:

$$g_k(\mathbf{Q}_G) = \frac{\exp(\mathbf{w}_k^\top \mathbf{Q}_G + b_k)}{\sum_{j=1}^K \exp(\mathbf{w}_j^\top \mathbf{Q}_G + b_j)}, \quad (3)$$

$$\sum_{k=1}^K g_k(\mathbf{Q}_G) = 1, \quad g_k(\mathbf{Q}_G) \geq 0, \quad (4)$$

where \mathbf{w}_k and b_k are the learnable parameters of the gating network for the k -th expert. This weighting reflects the relevance of the k -th expert for the input. The final vision embedding output \mathbf{v} is a weighted sum of the outputs from K experts:

$$\mathbf{v} = \sum_{k=1}^K g_k(\mathbf{Q}_G) \cdot a_k. \quad (5)$$

Text encoding: Given the L possible disease labels, each expressed as a textual prompt in the template of ‘a radiology image with [CLASS]’, we tokenize them and pass them through the frozen text encoder of the foundation VLM. We take the embedding of the end-of-text (EOT) token from the final layer of the text encoder, and project it using a learnable projection layer to align with the vision embedding space, producing L text features $\{\mathbf{z}_l\}_{l=1}^L$. When the paired clinical report r is available, we process it in the same manner as the label textual prompts.

Loss criterion: Let \mathbf{v} and $\{\mathbf{z}_l\}_{l=1}^L$ denote the MoE and the textual label features of embedding size f , respectively. We compute the cosine similarity between these via $\text{sim}(\mathbf{v}, \mathbf{z}_l) = \frac{\mathbf{v} \cdot \mathbf{z}_l}{\|\mathbf{v}\| \|\mathbf{z}_l\|}$, where $\|\cdot\|$ represents the L_2 norm. The resulting scores are treated as the predicted logits. Since medical images can be associated with multiple disease labels, we optimize a multi-label binary cross-entropy (BCE) loss, pushing similarities for present disease labels toward 1 and for absent ones toward 0. The same BCE loss is applied between the auxiliary clinical report features (when available) and the textual label features, providing additional supervision during adaptation.

4. Experimental Results

Datasets: We evaluated MedBridge and state-of-the-art adaptation approaches across five distinct medical imaging datasets: MIMIC-CXR v2 [14] ($n = 227k$), CheXpert Plus [3] ($n = 224k$), NIH ChestX-ray14 [35] ($n = 112k$), RSNA Pneumonia [30] ($n = 30k$), and COVIDx CXR-4 [38] ($n = 84k$). Among them, MIMIC-CXR, CheXpert Plus, and NIH ChestX-ray14 are multi-label datasets, where each subject may exhibit one or more of 14 common thoracic diseases. We evaluated the multi-label classification on all 14 observations. In contrast, RSNA Pneumonia consists of binary labels that distinguish normal cases from pneumonia, while COVIDx CXR-4 includes cases labeled either as no findings or COVID-19. In addition, MIMIC-CXR and CheXpert Plus also provide paired radiology reports. Further details are provided in Sec. A.1.

Evaluation metrics: We reported standard metrics for medical image classification: AUC score, macro-averaged F1 score, and accuracy (ACC). Following the best practice [28], the binary decision threshold was chosen to maximize the F1 score, and ACC was also calculated under this threshold. All metrics are macro-averaged over all disease classes present in the target dataset, reported in percentage (%). In addition, we show the computational efficiency of MedBridge and other baselines in Sec. A.3.

Baselines: We compared MedBridge with state-of-the-art adaptation methods for VLMs, including the zero-shot baseline with CLIP [25], prompt learning methods:

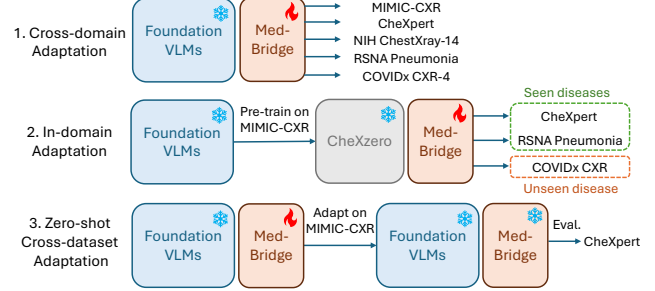


Figure 3. We evaluate MedBridge in three key adaptation tasks: (1) cross-domain adaptation: adapting foundation VLMs to medical data; (2) in-domain adaptation: adapting pre-trained medical VLMs to new datasets with seen and unseen diseases, and (3) zero-shot cross-dataset adaptation: after being adapted to a medical dataset, we test it on a new dataset without further fine-tuning.

CoOp [53], CoCoOp [52], ProGrad [55], KgCoOp [42], adapter-style learning methods: linear probing (LP) [25], CLIP-Adapter [7], MMA [41], MMRL [9], a low-rank adapter CLIP-LoRA [43], and a medical VLMs adaptation method abbreviated as LP + text [29]. These baseline methods were implemented using their official code.

Implementation details: We used the pre-trained CLIP model [25] with a ViT-B/16 backbone and 224×224 input resolution, as the standard foundation VLM for adaptation used for a fair comparison with baseline methods. For the MoE module, we add SigLIP [44] and a vision foundation model, DINOv2 [19], for efficiency. We further employed the pre-trained LLaVa-1.6 7B [18] and MedGemma-4B [27] models to evaluate the generalizability of MedBridge on different foundation VLMs. In the proposed Focal Sampling module, local regions were extracted at a size of 512×512 from the full-resolution image and resized to 224×224 as input. We used 10 focal inputs extracted using a sliding window with overlap. We used the AdamW optimizer at a learning rate of 5×10^{-4} and a batch size of 16, training for 3 epochs on a single NVIDIA H100 GPU.

4.1. Evaluation Tasks and Results

To comprehensively assess MedBridge’s adaptation capabilities, we conducted three key evaluations shown in Fig. 3:

- **Cross-domain adaptation:** We directly adapted general-purpose VLMs to medical data for disease diagnosis, simulating the challenging task of transferring knowledge from non-medical to medical domains.
- **In-domain adaptation:** We evaluated how well VLMs, already pre-trained on large-scale medical data (e.g., CheXzero [33]), can adapt to new medical datasets, covering both previously seen and unseen disease scenarios.
- **Zero-shot cross-dataset evaluation:** We examined a domain generalization adaptation scenario, in which we first adapted general-purpose VLMs to the medical domain

Table 1. Evaluation of *cross-domain adaptation* on five medical datasets test sets. Complete results are reported in Tab. A.1.

Method	CheXpert Plus [3]		MIMIC-CXR [14]		NIH CXR-14 [35]		RSNA Pneu. [30]		COVIDx CXR-4 [38]	
	AUC \uparrow	ACC \uparrow	AUC \uparrow	ACC \uparrow	AUC \uparrow	ACC \uparrow	AUC \uparrow	ACC \uparrow	AUC \uparrow	ACC \uparrow
CLIP (ICML2021) [25]	51.07	19.65	51.74	13.46	50.11	9.65	38.98	22.98	50.74	50.00
CoOp (IJCV2022) [53]	66.66	68.16	63.69	70.96	57.98	61.43	82.10	76.91	56.89	50.54
CoCoOp (CVPR2022) [52]	61.50	65.62	59.86	54.80	52.12	36.87	81.58	76.05	56.16	50.01
ProGrad (ICCV2023) [55]	61.93	62.02	58.91	53.51	52.89	38.35	81.23	77.55	54.18	50.67
KgCoOp (CVPR2023) [42]	64.29	64.51	60.55	64.53	55.08	48.76	77.43	72.94	57.10	50.85
Linear Probing (ICML2021) [25]	68.45	71.48	65.20	68.87	58.22	57.59	81.39	77.96	58.31	51.27
LP + text (MICCAI2024) [29]	51.87	19.65	53.28	13.46	56.65	32.65	50.00	77.02	55.31	50.00
CLIP-Adapter (IJCV2024) [7]	62.24	60.52	57.20	49.63	51.00	33.45	78.46	73.16	58.87	50.09
CLIP-LoRA (CVPRW2024) [43]	75.91	82.13	66.30	72.05	59.90	50.17	84.63	79.01	62.15	53.53
MMA (CVPR2024) [41]	74.76	80.76	64.03	65.44	57.83	47.99	81.86	76.76	65.06	53.20
MMRL (CVPR2025) [9]	76.46	80.68	64.74	65.03	60.79	66.71	82.14	76.01	66.90	55.88
MedBridge	81.49	<u>85.01</u>	70.59	76.41	<u>65.03</u>	69.70	<u>85.38</u>	<u>79.35</u>	<u>73.81</u>	<u>67.44</u>
MedBridge (w/ report)	81.69	85.58	<u>72.01</u>	77.89	-	-	-	-	-	-
MedBridge (w/ MoE)	83.55	83.62	<u>71.92</u>	<u>77.84</u>	66.42	<u>69.58</u>	86.26	79.50	76.37	70.51
MedBridge (w/ report & MoE)	<u>83.28</u>	82.49	72.03	77.26	-	-	-	-	-	-

Table 2. AUC scores (%) of *cross-domain adaptation* on test sets under different training data portions.

Task	Cross-Domain Adaptation															
	Dataset				CheXpert Plus				RSNA Pneumonia				COVIDx CXR-4			
Data Portion	1%	10%	50%	100%	1%	10%	50%	100%	1%	10%	50%	100%	1%	10%	50%	100%
CoOp (IJCV2022)	56.79	65.83	69.95	66.66	<u>74.70</u>	<u>79.04</u>	<u>81.41</u>	82.10	36.15	56.44	58.02	56.89	<u>58.42</u>	<u>57.62</u>	<u>57.78</u>	64.29
KgCoOp (CVPR2023)	<u>58.42</u>	57.62	57.78	64.29	62.86	67.74	69.29	77.43	38.44	53.29	54.99	57.10	58.22	66.30	68.98	68.45
LP (ICML2021)	58.22	66.30	68.98	68.45	73.01	78.14	80.60	81.39	<u>62.63</u>	59.09	59.51	58.31	49.23	60.63	72.82	77.46
CLIP-LoRA (CVPRW2024)	49.23	60.63	72.82	77.46	62.20	69.56	80.21	<u>84.63</u>	61.87	<u>61.46</u>	63.68	62.15	49.58	<u>68.96</u>	76.33	74.76
MMA (CVPR2024)	49.58	<u>68.96</u>	76.33	74.76	33.05	58.08	81.29	81.86	55.37	61.35	<u>71.68</u>	65.06	58.71	66.80	<u>76.74</u>	<u>76.46</u>
MedBridge (ours)	64.52	69.64	77.22	81.49	76.27	79.84	84.16	85.38	67.75	74.42	76.14	73.81				

using a public medical dataset, then directly performed zero-shot multi-label classification on a different dataset without further fine-tuning.

For both cross- and in-domain adaptation settings, we evaluated performance under varying amounts of labeled training data (1%, 10%, 50%, and 100%) to simulate real-world clinical scenarios with different levels of data availability. Unless stated otherwise, the reported results of MedBridge are without clinical reports or MoE during adaptation to ensure a fair comparison with baseline methods.

4.1.1. Cross-Domain Adaptation

Here, we used frozen CLIP models pre-trained on large-scale natural image-text pairs as representative foundation VLMs, and adapted them with MedBridge and state-of-the-art multimodal adaptation approaches on multi-label thoracic disease classification across five medical datasets. Sec. 4.1.4 reports the performance of MedBridge using other foundation VLMs. To save space, most of the results are shown in Tab. 1 and the complete results are provided

in Tab. A.1. According to the tables, zero-shot classification using the pre-trained CLIP achieved only around 51% AUC on average, highlighting the significant domain gap between natural and medical images and the need for effective adaptation. Existing adaptation methods substantially improved performance, with CLIP-LoRA achieving an AUC of 75.91% and MMRL achieving 76.46% on CheXpert Plus. MedBridge further increased accuracy, outperforming MMRL by more than 7% on the CheXpert Plus, MIMIC-CXR, and COVIDx CXR-4 datasets, and by approximately 5% on NIH and RSNA Pneumonia, demonstrating its superior generalization and diagnostic performance. The addition of the MoE module to MedBridge further improved its diagnostic precision, especially in CheXpert Plus and COVIDx CXR-4, increasing AUC by 2% and 2.5%, respectively. Integrating auxiliary clinical reports into MIMIC-CXR during adaptation further enhanced its AUC by 1.5%. In addition, as shown in Tab. 2, MedBridge maintained consistently high performance across different training data proportions, highlighting its strong data efficiency.

Table 3. AUC scores (%) of *in-domain adaptation* with CheXzero on the test sets under different training data portions.

Dataset	CheXpert Plus (Seen Disease)				COVIDx CXR-4 (Unseen Disease)			
	1%	10%	50%	100%	1%	10%	50%	100%
CoOp	58.5	64.9	70.3	72.1	50.6	55.4	57.6	56.6
KgCoOp	59.9	64.1	64.9	64.5	42.9	53.8	54.3	58.6
LP	64.3	64.8	74.2	83.3	60.1	61.6	65.5	65.7
CLIP-LoRA	58.2	65.0	77.8	81.5	52.3	58.6	71.1	71.0
MMA	49.2	73.6	77.7	77.9	50.9	60.8	65.2	69.4
MMRL	59.4	69.6	76.5	80.7	<u>62.6</u>	<u>66.5</u>	67.1	<u>73.4</u>
MedBridge	68.1	<u>71.5</u>	78.3	86.6	72.9	73.6	75.2	78.1

4.1.2. In-Domain Adaptation

We also assessed the ability of MedBridge and other adaptation methods to adapt in-domain pre-trained VLMs, i.e., VLMs that have already been further pre-trained on medical datasets, to new medical datasets for diagnosing both previously seen and unseen diseases. To this end, we used CheXzero [33], a self-supervised CLIP-based model pre-trained on the MIMIC-CXR dataset [14]. Since the diseases in CheXpert Plus are also present in MIMIC-CXR, we used them to assess in-domain adaptation on seen diseases. In contrast, COVID-19 represents an unseen disease for the CheXzero model, thus, we utilized the COVIDx CXR-4 dataset to evaluate in-domain adaptation to unseen disease. We also investigated performance under varying amounts of labeled training data. Tab. 3 reported the performance of MedBridge and six best-performed adaptation baselines. In-domain adaptation achieved an overall higher diagnostic accuracy compared to cross-domain adaptation due to the reduced domain gap. Existing adaptation methods performed well for the in-domain adaptation with seen diseases, i.e., CheXpert, as they were primarily designed for in-domain use. MedBridge achieved comparably high performance on the seen diseases. Notably, in the case of the unseen disease (COVID-19), MedBridge achieved a significantly higher performance, with an AUC score of 78.1%, outperforming the second-best adaptation method by 5% while maintaining stable results across varying training data proportions. Given the common data scarcity in the medical domain, this setting reflects real-world needs for rapid adaptation to emerging diseases, highlighting the efficiency and practical utility of MedBridge in clinical applications.

4.1.3. Zero-Shot Cross-Dataset Evaluation

We assessed the zero-shot cross-dataset adaptation capability of MedBridge by first adapting the foundation VLM to the medical domain using the large-scale MIMIC-CXR dataset, aiming to narrow the domain gap between natural and medical images. We then conducted zero-shot multi-label classification on the CheXpert Plus dataset, without further fine-tuning. As presented in Tab. 4, MedBridge

Table 4. Comparisons with SOTA adaptation methods under zero-shot cross-dataset classification on the test sets.

Method	Source	Target		
	MIMIC	CheXpert Plus		
		AUC↑	AUC↑	F1↑
CoOp [53]	63.69	69.34	38.72	77.15
CoCoOp [52]	59.86	64.81	37.76	70.27
ProGrad [55]	58.91	60.06	34.14	62.80
KgCoOp [42]	60.55	65.29	36.55	72.46
LP [25]	65.20	73.66	40.55	76.31
CLIP-Ad. [7]	57.20	63.92	36.50	71.10
CLIP-LoRA [43]	66.30	74.80	44.80	<u>84.82</u>
MMA [41]	64.03	76.07	<u>46.84</u>	83.78
MMRL [9]	64.74	76.48	45.20	82.38
MedBridge	<u>70.59</u>	<u>78.69</u>	45.01	84.78
MedB. (w/ MoE)	71.92	79.94	47.15	85.12

substantially outperformed state-of-the-art adaptation methods, achieving the highest AUC of 79.94%, which is nearly 3.5% higher than the next best method, MMRL. It indicates the effectiveness of MedBridge in improving generalization across diverse medical datasets, where foundation VLMs can be tuned on public datasets and then reliably deployed in data-limited local clinical settings.

4.1.4. Adaptation of Various Foundation VLMs

To ensure a fair comparison with baseline methods, we used CLIP as the foundation VLM in the previous sections. However, MedBridge is highly versatile and designed to be VLM-agnostic. It can readily adapt different foundation VLMs with their respective visual and text encoders, such as MedGemma [27] for in-domain adaptation, and LLaVa [18] for cross-domain adaptation. As shown in Tab. 5, MedBridge successfully adapted these VLM backbones across CheXpert Plus, MIMIC-CXR, and RSNA Pneumonia datasets, outperforming their original performance by a large margin. We observed sequential performance gains, starting from CLIP and increasing with the larger LLaVa foundation model. The best results were achieved with the domain-specific MedGemma backbone, yielding the highest AUC of 85.83% in CheXpert Plus, 76.88% in MIMIC-CXR, and 89.68% in RSNA Pneumonia. It demonstrates the effectiveness and generalizability of MedBridge across diverse foundation VLMs.

4.2. Ablation Study

We performed comprehensive ablation studies to evaluate key designs in MedBridge, including the MoE, the Focal Sampling module, the QEncoder with its weighting factor α , and the backbone sizes. We reported the average AUC on the *validation sets* of three representative datasets: CheXpert Plus, MIMIC-CXR, and RSNA Pneumonia, with detailed and additional ablation results provided in Sec. A.5.

Table 5. Evaluation of Medbridge with different foundation VLMs on three medical *test* sets. Complete results are reported in Tab. A.4.

Adaptation	Method	CheXpert Plus [3]			MIMIC-CXR [14]			RSNA Pneumonia [30]		
		AUC \uparrow	F1 \uparrow	ACC \uparrow	AUC \uparrow	F1 \uparrow	ACC \uparrow	AUC \uparrow	F1 \uparrow	ACC \uparrow
Cross-domain	CLIP	51.07	28.85	19.65	51.74	22.40	13.46	38.98	37.37	22.98
	LLaVa	52.07	31.50	46.80	48.14	22.64	27.40	48.72	37.32	22.94
	MedBridge (CLIP)	81.49	47.30	85.01	70.59	33.04	76.41	85.38	62.08	79.35
	MedBridge (LLaVA)	84.49	50.41	84.65	73.57	35.56	77.97	86.49	64.72	80.55
In-domain	MedGemma	52.66	30.37	48.97	53.75	25.09	38.18	59.40	38.81	39.13
	MedBridge (MedGemma)	85.83	56.06	85.34	76.88	38.19	81.69	89.68	70.11	85.46

MoE Module: Tab. 6 shows the impact of the MoE module and the inclusion of different foundation models for disease diagnosis. While using CLIP alone provided a baseline with an AUC of 85.08% in RSNA Pneumonia and 75.41% in CheXpert Plus, the inclusion of additional, larger-scale, and more specialized experts substantially improved performance in both datasets. For the RSNA dataset, the AUC improved to 86.95% in the cross-domain setting (adding LLaVA and MetaCLIP) and further to 89.14% in the in-domain setting (adding LLaVA and MedGemma). Performance on CheXpert Plus also increased significantly to an AUC of 80.65%. Detailed results are provided in Tab. A.8.

Focal Sampling: Fig. 4a explored the impact of incorporating varying numbers of fine-grained inputs in the Focal Sampling module. Two strategies are reported: randomly sampling the local regions or systematically extracting them using a sliding window with overlap. Using only the whole resized image (no focal input) yielded the lowest performance, while adding more focal inputs improved accuracy. **QEncoder:** Fig. 4b illustrates the effect of varying the number of learnable query tokens (Q) generated by QEncoders. Detailed results are provided in Sec. A.5. Considering a 1% margin from the performance peak, Q in the range of [24, 36] yields improved results, corresponding to approximately 10–18% of the frozen tokens. Furthermore, Tab A.9 demonstrates that employing a shallow-to-moderate injection depth (e.g., $n_2 = 3$) provides the best trade-off between diagnostic accuracy and computational efficiency.

Weighting factor α : This constant hyperparameter controls the relative contribution of the learnable queries generated

Table 6. Ablation on different experts in the MoE module on the validation sets. Detailed results are reported in Tab. A.8.

Experts	RSNA Pneumonia		CheXpert Plus	
	AUC \uparrow	ACC \uparrow	AUC \uparrow	ACC \uparrow
CLIP	85.08	78.31	75.41	75.64
CLIP + SigLIP	85.98	79.20	76.25	77.48
CLIP + SigLIP + DINOv2	86.26	82.84	76.44	76.27
CLIP + EVA-CLIP	86.66	82.13	76.87	77.86
CLIP + LLaVa	86.69	82.02	77.97	79.28
CLIP + LLaVa + MetaCLIP	86.95	81.60	77.56	78.22
CLIP + MedGemma	88.50	83.06	78.61	77.23
CLIP + LLaVa + MedGemma	89.26	83.48	80.65	79.95

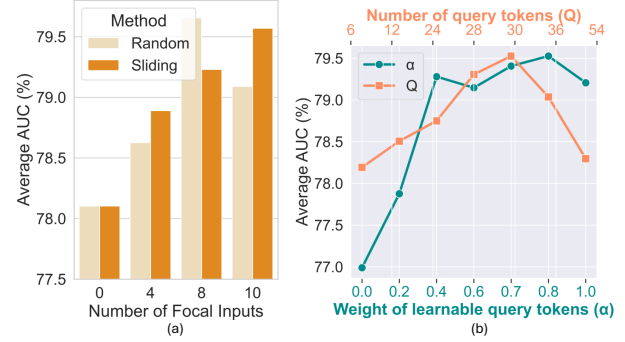


Figure 4. Ablation on (a) the Focal Sampling module and (b) the number Q and weight α of query tokens in the QEncoder.

by the QEncoders in the diagnosis. As shown in Fig. 4b, values of α within the range [0.4, 1.0] yield stable performance, while a near-zero value, indicating a minimal contribution, leads to a substantial drop in AUC for 2.5%.

Backbone size: For a fair comparison with other methods, we used the baseline ViT-Base in all experiments. Sec. A.5 further evaluated the size of ViT backbones ranging from Small to Huge, showing that performance improved consistently with larger model size. Specifically, the AUC increases by 1.7% from ViT-Small to ViT-Huge on the RSNA Pneumonia dataset, demonstrating that MedBridge scales effectively with larger VLMs.

5. Discussion and Conclusion

We introduced MedBridge, a lightweight domain adaptation framework designed to flexibly adapt different foundation VLMs for accurate diagnosis in chest X-rays. While medical vision-language pretraining typically takes several days on multiple GPUs [33], MedBridge completes adaptation in just a few hours with one single GPU (Sec. A.3). Across five medical datasets in three key evaluations: cross-domain, in-domain, and zero-shot cross-dataset adaptation, MedBridge consistently outperforms diverse adaptation strategies in accuracy, data efficiency, and generalization. This performance gain is largely due to its effective use of learnable query tokens and expert foundation models with the capability to capture pathological cues from fine-grained regions. In addition, MedBridge is highly versatile and can readily adapt arbitrary foundation VLMs, with performance scaling effectively when integrating larger, more specialized

models, such as LLaVa and MedGemma. While the addition of multiple experts and focal sampling increases training time compared to other adapters, it still requires only a fraction of the resources for original VLM training.

Acknowledgements

This work was supported by the Munich Center for Machine Learning (MCML), the German Research Foundation (DFG), and the DAAD programme Konrad Zuse Schools of Excellence in Artificial Intelligence, sponsored by the Federal Ministry of Research, Technology and Space. The authors gratefully acknowledge the scientific support and resources of the AI service infrastructure LRZ AI Systems provided by the Leibniz Supercomputing Centre (LRZ) of the Bavarian Academy of Sciences and Humanities (BAdW), funded by Bayerisches Staatsministerium für Wissenschaft und Kunst (StMWK).

References

[1] Anas Awadalla, Irena Gao, Josh Gardner, Jack Hessel, Yusuf Hanafy, Wanrong Zhu, Kalyani Marathe, Yonatan Bitton, Samir Gadre, Shiori Sagawa, et al. Openflamingo: An open-source framework for training large autoregressive vision-language models. *arXiv preprint arXiv:2308.01390*, 2023. 1

[2] Jimmy Lei Ba, Jamie Ryan Kiros, and Geoffrey E Hinton. Layer normalization. *arXiv preprint arXiv:1607.06450*, 2016. 3

[3] Pierre Chambon, Jean-Benoit Delbrouck, Thomas Sounack, Shih-Cheng Huang, Zhihong Chen, Maya Varma, Steven QH Truong, Chu The Chuong, and Curtis P Langlotz. Chexpert plus: Augmenting a large chest x-ray dataset with text radiology reports, patient demographics and additional image formats. *arXiv preprint arXiv:2405.19538*, 2024. 5, 6, 8

[4] Pierre Joseph Marcel Chambon, Christian Bluethgen, Curtis Langlotz, and Akshay Chaudhari. Adapting pretrained vision-language foundational models to medical imaging domains. In *NeurIPS 2022 Foundation Models for Decision Making Workshop*. 3

[5] Cheng Cheng, Lin Song, Ruoyi Xue, Hang Wang, Hongbin Sun, Yixiao Ge, and Ying Shan. Meta-adapter: an online few-shot learner for vision-language model. In *Proceedings of the 37th International Conference on Neural Information Processing Systems*, pages 55361–55374, 2023. 1

[6] Mehdi Cherti, Romain Beaumont, Ross Wightman, Mitchell Wortsman, Gabriel Ilharco, Cade Gordon, Christoph Schuhmann, Ludwig Schmidt, and Jenia Jitsev. Reproducible scaling laws for contrastive language-image learning. In *Proceedings of the IEEE/CVF conference on computer vision and pattern recognition*, pages 2818–2829, 2023. 1, 2

[7] Peng Gao, Shijie Geng, Renrui Zhang, Teli Ma, Rongyao Fang, Yongfeng Zhang, Hongsheng Li, and Yu Qiao. Clip-adapter: Better vision-language models with feature adapters. *International Journal of Computer Vision*, 132(2): 581–595, 2024. 1, 2, 5, 6, 7

[8] Team Gemini. Gemini: A family of highly capable multi-modal models. *arXiv preprint arXiv:2312.11805*, 2023. 2

[9] Yuncheng Guo and Xiaodong Gu. Mmrl: Multi-modal representation learning for vision-language models. In *Proceedings of the IEEE/CVF Conference on Computer Vision and Pattern Recognition*, 2025. 1, 2, 5, 6, 7

[10] Gregory Holste, Yiliang Zhou, Song Wang, Ajay Jaiswal, Mingquan Lin, Sherry Zhuge, Yuzhe Yang, Dongkyun Kim, Trong-Hieu Nguyen-Mau, Minh-Triet Tran, et al. Towards long-tailed, multi-label disease classification from chest x-ray: Overview of the cxr-it challenge. *Medical Image Analysis*, page 103224, 2024. 1

[11] Chaoqin Huang, Aofan Jiang, Jinghao Feng, Ya Zhang, Xinchao Wang, and Yanfeng Wang. Adapting visual-language models for generalizable anomaly detection in medical images. In *Proceedings of the IEEE/CVF Conference on Computer Vision and Pattern Recognition*, pages 11375–11385, 2024. 1, 3

[12] Shih-Cheng Huang, Liyue Shen, Matthew P Lungren, and Serena Yeung. Gloria: A multimodal global-local representation learning framework for label-efficient medical image recognition. In *Proceedings of the IEEE/CVF international conference on computer vision*, pages 3942–3951, 2021. 3

[13] Chao Jia, Yinfei Yang, Ye Xia, Yi-Ting Chen, Zarana Parekh, Hieu Pham, Quoc Le, Yun-Hsuan Sung, Zhen Li, and Tom Duerig. Scaling up visual and vision-language representation learning with noisy text supervision. In *Proceedings of the 38th International Conference on Machine Learning*, pages 4904–4916. PMLR, 2021. 1

[14] Alistair EW Johnson, Tom J Pollard, Seth J Berkowitz, Nathaniel R Greenbaum, Matthew P Lungren, Chih-ying Deng, Roger G Mark, and Steven Horng. Mimic-cxr, a de-identified publicly available database of chest radiographs with free-text reports. *Scientific data*, 6(1):317, 2019. 5, 6, 7, 8

[15] Junnan Li, Dongxu Li, Silvio Savarese, and Steven Hoi. Blip-2: Bootstrapping language-image pre-training with frozen image encoders and large language models. In *International conference on machine learning*, pages 19730–19742. PMLR, 2023. 3

[16] Chenyu Lian, Hong-Yu Zhou, Yizhou Yu, and Liansheng Wang. Less could be better: Parameter-efficient fine-tuning advances medical vision foundation models. In *Medical Imaging with Deep Learning*, 2024. 3

[17] Aixin Liu, Bei Feng, Bing Xue, Bingxuan Wang, Bochao Wu, Chengda Lu, Chenggang Zhao, Chengqi Deng, Chenyu Zhang, Chong Ruan, et al. Deepseek-v3 technical report. *arXiv preprint arXiv:2412.19437*, 2024. 1

[18] Haotian Liu, Chunyuan Li, Yuhang Li, and Yong Jae Lee. Visual instruction tuning. *arXiv preprint arXiv:2304.08485*, 2023. 1, 2, 5, 7

[19] Maxime Oquab, Timothée Darcet, Théo Moutakanni, Huy V Vo, Marc Szafraniec, Vasil Khalidov, Pierre Fernandez, Daniel HAZIZA, Francisco Massa, Alaaeldin El-Nouby, et al. Dinov2: Learning robust visual features without supervision. *Transactions on Machine Learning Research*, 2024. 5

[20] Chantal Pellegrini, Ege Özsoy, Benjamin Busam, Benedikt Wiestler, Nassir Navab, and Matthias Keicher. Radiolog: Large vision-language models for x-ray reporting and dialog-driven assistance. In *Medical Imaging with Deep Learning*, 2025. 3

[21] Fernando Pérez-García, Harshita Sharma, Sam Bond-Taylor, Kenza Bouzid, Valentina Salvatelli, Maximilian Ilse, Shruthi Bannur, Daniel C Castro, Anton Schwaighofer, Matthew P Lungren, et al. Exploring scalable medical image encoders beyond text supervision. *Nature Machine Intelligence*, pages 1–12, 2025. 3

[22] Vu Minh Hieu Phan, Yutong Xie, Yuankai Qi, Lingqiao Liu, Liyang Liu, Bowen Zhang, Zhibin Liao, Qi Wu, Minh-Son To, and Johan W Verjans. Decomposing disease descriptions for enhanced pathology detection: A multi-aspect vision-language pre-training framework. In *Proceedings of the IEEE/CVF Conference on Computer Vision and Pattern Recognition*, pages 11492–11501, 2024. 3

[23] Kanchan Poudel, Manish Dhakal, Prasiddha Bhandari, Rabin Adhikari, Safal Thapaliya, and Bishesh Khanal. Ex-

ploring transfer learning in medical image segmentation using vision-language models. In *Medical Imaging with Deep Learning*, pages 1142–1165. PMLR, 2024. 1, 3

[24] Ziyuan Qin, Huahui Yi, Qicheng Lao, and Kang Li. Medical image understanding with pretrained vision language models: A comprehensive study. In *The Eleventh International Conference on Learning Representations*. 1, 3

[25] Alec Radford, Jong Wook Kim, Chris Hallacy, Aditya Ramesh, Gabriel Goh, Sandhini Agarwal, Girish Sastry, Amanda Askell, Pamela Mishkin, Jack Clark, et al. Learning transferable visual models from natural language supervision. In *International conference on machine learning*, pages 8748–8763. PMLR, 2021. 1, 2, 5, 6, 7

[26] Christoph Schuhmann, Romain Beaumont, Richard Vencu, Cade Gordon, Ross Wightman, Mehdi Cherti, Theo Coombes, Aarush Katta, Clayton Mullis, Mitchell Wortsman, et al. Laion-5b: An open large-scale dataset for training next generation image-text models. *Advances in neural information processing systems*, 35:25278–25294, 2022. 2

[27] Andrew Sellergren, Sahar Kazemzadeh, Tiam Jaroensri, Atilla Kiraly, Madeleine Traverse, Timo Kohlberger, Shawn Xu, Fayaz Jamil, Cian Hughes, Charles Lau, et al. Medgemma technical report. *arXiv preprint arXiv:2507.05201*, 2025. 2, 3, 5, 7

[28] Laleh Seyyed-Kalantari, Haoran Zhang, Matthew BA McDermott, Irene Y Chen, and Marzyeh Ghassemi. Under-diagnosis bias of artificial intelligence algorithms applied to chest radiographs in under-served patient populations. *Nature medicine*, 27(12):2176–2182, 2021. 5

[29] Fereshteh Shakeri, Yunshi Huang, Julio Silva-Rodríguez, Houda Bahig, An Tang, Jose Dolz, and Ismail Ben Ayed. Few-shot adaptation of medical vision-language models. In *International Conference on Medical Image Computing and Computer-Assisted Intervention*, pages 553–563. Springer, 2024. 2, 3, 5, 6

[30] George Shih, Carol C Wu, Safwan S Halabi, Marc D Kohli, Luciano M Prevedello, Tessa S Cook, Arjun Sharma, Judith K Amorosa, Veronica Arteaga, Maya Galperin-Aizenberg, et al. Augmenting the national institutes of health chest radiograph dataset with expert annotations of possible pneumonia. *Radiology: Artificial Intelligence*, 1(1):e180041, 2019. 5, 6, 8

[31] Hao-Zhe Tan, Zhi Zhou, Yu-feng Li, and Lan-Zhe Guo. Vision-language model selection and reuse for downstream adaptation. In *Forty-second International Conference on Machine Learning*, 2025. 1

[32] Gemma Team, Thomas Mesnard, Cassidy Hardin, Robert Dadashi, Surya Bhupatiraju, Shreya Pathak, Laurent Sifre, Morgane Rivière, Mihir Sanjay Kale, Juliette Love, et al. Gemma: Open models based on gemini research and technology. *arXiv preprint arXiv:2403.08295*, 2024. 2

[33] Ekin Tiu, Ellie Talius, Pujan Patel, Curtis P Langlotz, Andrew Y Ng, and Pranav Rajpurkar. Expert-level detection of pathologies from unannotated chest x-ray images via self-supervised learning. *Nature biomedical engineering*, 6(12):1399–1406, 2022. 2, 3, 5, 7, 8

[34] Fuying Wang, Yuyin Zhou, Shujun Wang, Varut Vardhanabutti, and Lequan Yu. Multi-granularity cross-modal alignment for generalized medical visual representation learning. *Advances in Neural Information Processing Systems*, 35:33536–33549, 2022. 3

[35] Xiaosong Wang, Yifan Peng, Le Lu, Zhiyong Lu, Mohammad Bagheri, and Ronald M Summers. Chestx-ray8: Hospital-scale chest x-ray database and benchmarks on weakly-supervised classification and localization of common thorax diseases. In *Proceedings of the IEEE conference on computer vision and pattern recognition*, pages 2097–2106, 2017. 5, 6

[36] Zifeng Wang, Zhenbang Wu, Dinesh Agarwal, and Jimeng Sun. Medclip: Contrastive learning from unpaired medical images and text. In *Proceedings of the Conference on Empirical Methods in Natural Language Processing. Conference on Empirical Methods in Natural Language Processing*, page 3876, 2022. 3

[37] Chaoyi Wu, Xiaoman Zhang, Ya Zhang, Yanfeng Wang, and Weidi Xie. Medclip: Medical knowledge enhanced language-image pre-training for x-ray diagnosis. In *Proceedings of the IEEE/CVF International Conference on Computer Vision*, pages 21372–21383, 2023. 3

[38] Yifan Wu, Hayden Gunraj, Chi-en Amy Tai, and Alexander Wong. Covidx cxr-4: An expanded multi-institutional open-source benchmark dataset for chest x-ray image-based computer-aided covid-19 diagnostics. *arXiv preprint arXiv:2311.17677*, 2023. 5, 6

[39] Shin’ya Yamaguchi, Dewei Feng, Sekitoshi Kanai, Kazuki Adachi, and Daiki Chijiwa. Post-pre-training for modality alignment in vision-language foundation models. In *Proceedings of the IEEE/CVF Conference on Computer Vision and Pattern Recognition*, 2025. 1

[40] An Yang, Baosong Yang, Beichen Zhang, Binyuan Hui, Bo Zheng, Bowen Yu, Chengyuan Li, Dayiheng Liu, Fei Huang, Haoran Wei, et al. Qwen2. 5 technical report. *arXiv preprint arXiv:2412.15115*, 2024. 1

[41] Lingxiao Yang, Ru-Yuan Zhang, Yanchen Wang, and Xiaohua Xie. Mma: Multi-modal adapter for vision-language models. In *Proceedings of the IEEE/CVF Conference on Computer Vision and Pattern Recognition*, pages 23826–23837, 2024. 1, 2, 5, 6, 7

[42] Hantao Yao, Rui Zhang, and Changsheng Xu. Visual-language prompt tuning with knowledge-guided context optimization. In *Proceedings of the IEEE/CVF conference on computer vision and pattern recognition*, pages 6757–6767, 2023. 1, 2, 5, 6, 7

[43] Maxime Zanella and Ismail Ben Ayed. Low-rank few-shot adaptation of vision-language models. In *Proceedings of the IEEE/CVF Conference on Computer Vision and Pattern Recognition*, pages 1593–1603, 2024. 2, 5, 6, 7

[44] Xiaohua Zhai, Basil Mustafa, Alexander Kolesnikov, and Lucas Beyer. Sigmoid loss for language image pre-training. In *Proceedings of the IEEE/CVF international conference on computer vision*, pages 11975–11986, 2023. 1, 2, 5

[45] Jiajin Zhang, Ge Wang, Mannudeep K Kalra, and Pingkun Yan. Disease-informed adaptation of vision-language models. *IEEE Transactions on Medical Imaging*, 2024. 3

[46] Renrui Zhang, Wei Zhang, Rongyao Fang, Peng Gao, Kun-chang Li, Jifeng Dai, Yu Qiao, and Hongsheng Li. Tip-

adapter: Training-free adaption of clip for few-shot classification. In *Computer Vision – ECCV 2022: 17th European Conference, Tel Aviv, Israel, October 23–27, 2022, Proceedings, Part XXXV*, page 493–510. Springer-Verlag, 2022. [2](#)

[47] Xiaoman Zhang, Chaoyi Wu, Ya Zhang, Weidi Xie, and Yanfeng Wang. Knowledge-enhanced visual-language pre-training on chest radiology images. *Nature Communications*, 14(1):4542, 2023. [3](#)

[48] Ximiao Zhang, Min Xu, Dehui Qiu, Ruixin Yan, Ning Lang, and Xiuzhuang Zhou. Mediclip: Adapting clip for few-shot medical image anomaly detection. In *International Conference on Medical Image Computing and Computer-Assisted Intervention*, pages 458–468. Springer, 2024. [1, 3](#)

[49] Yuhui Zhang, Shih-Cheng Huang, Zhengping Zhou, Matthew P Lungren, and Serena Yeung. Adapting pre-trained vision transformers from 2d to 3d through weight inflation improves medical image segmentation. In *Machine Learning for Health*, pages 391–404. PMLR, 2022. [1, 3](#)

[50] Yuhao Zhang, Hang Jiang, Yasuhide Miura, Christopher D Manning, and Curtis P Langlotz. Contrastive learning of medical visual representations from paired images and text. In *Machine learning for healthcare conference*, pages 2–25. PMLR, 2022. [3](#)

[51] Zihao Zhao, Yuxiao Liu, Han Wu, Mei Wang, Yonghao Li, Sheng Wang, Lin Teng, Disheng Liu, Zhiming Cui, Qian Wang, et al. Clip in medical imaging: A survey. *Medical Image Analysis*, page 103551, 2025. [2](#)

[52] Kaiyang Zhou, Jingkang Yang, Chen Change Loy, and Ziwei Liu. Conditional prompt learning for vision-language models. In *Proceedings of the IEEE/CVF conference on computer vision and pattern recognition*, pages 16816–16825, 2022. [1, 2, 5, 6, 7](#)

[53] Kaiyang Zhou, Jingkang Yang, Chen Change Loy, and Ziwei Liu. Learning to prompt for vision-language models. *International Journal of Computer Vision*, 130(9):2337–2348, 2022. [1, 2, 5, 6, 7](#)

[54] Yang Zhou, Tan Faith, Yanyu Xu, Sicong Leng, Xinxing Xu, Yong Liu, and Rick Siow Mong Goh. Benchx: A unified benchmark framework for medical vision-language pretraining on chest x-rays. *Advances in Neural Information Processing Systems*, 37:6625–6647, 2024. [3](#)

[55] Beier Zhu, Yulei Niu, Yucheng Han, Yue Wu, and Hanwang Zhang. Prompt-aligned gradient for prompt tuning. In *Proceedings of the IEEE/CVF international conference on computer vision*, pages 15659–15669, 2023. [1, 2, 5, 6, 7](#)